

LOW-MASS AGN AND THEIR RELATION TO THE FUNDAMENTAL PLANE OF BLACK HOLE ACCRETION

KAYHAN GÜLTEKIN¹, EDWARD M. CACKETT², ASHLEY L. KING¹, JON M. MILLER¹, AND JASON PINKNEY³

¹Department of Astronomy, University of Michigan, 500 Church Street, Ann Arbor, MI 48109, USA; kayhan@umich.edu

²Department of Physics and Astronomy, Wayne State University, 666 West Hancock Street, Detroit, MI 48201, USA and

³Department of Physics and Astronomy, Ohio Northern University, 525 S. Main St., Ada, OH 45810, USA

Accepted by The Astrophysical Journal Letters

ABSTRACT

We put active galactic nuclei (AGNs) with low-mass black holes on the fundamental plane of black hole accretion—the plane that relates X-ray emission, radio emission, and mass of an accreting black hole—to test whether or not the relation is universal for both stellar-mass and supermassive black holes. We use new *Chandra* X-ray and Very Large Array radio observations of a sample of black holes with masses less than $10^{6.3} M_{\odot}$, which have the best leverage for determining whether supermassive black holes and stellar-mass black holes belong on the same plane. Our results suggest that the two different classes of black holes both belong on the same relation. These results allow us to conclude that the fundamental plane is suitable for use in estimating supermassive black hole masses smaller than $\sim 10^7 M_{\odot}$, in testing for intermediate-mass black holes, and in estimating masses at high accretion rates.

Subject headings: accretion, accretion disks — black hole physics — galaxies: active — galaxies: jets — radio continuum: galaxies — X-rays: galaxies

1. INTRODUCTION

The continuum X-ray and radio emission and mass of accreting black holes are empirically correlated (Merloni et al. 2003; Falcke et al. 2004). The correlation, frequently called the “fundamental plane of black hole accretion,” relates mass accretion rates, probed by the X-ray luminosity, and jet or outflow power, probed by the radio luminosity, at a given mass of the black hole, which sets the size scale of the accretion-disk–jet system. The relation was first seen in stellar-mass black holes, which have a narrow range in mass (Gallo et al. 2003), and then extended to all black holes (Merloni et al. 2003; Falcke et al. 2004), covering over 8 orders of magnitude in mass, 14 orders of magnitude in radio luminosity, and 12 orders of magnitude in X-ray luminosity.

Despite the wide range that the fundamental plane covers, there is room to question its universality. For example, using a larger sample of stellar-mass black hole data, Gallo et al. (2012) found that the radio–X-ray correlation was best explained by two tracks, with one source that transitions from one track to the other. Restricting to only black holes with dynamical mass measurements, Gültekin et al. (2009) found different results when including and excluding stellar-mass black holes ($L_R \sim M^{0.78} L_X^{0.67}$ and $L_R \sim M^{2.08} L_X^{0.50}$, respectively).

There are two potential explanations for the separate relations found by Gültekin et al. (2009). The first is that supermassive black holes (SMBHs) and stellar-mass black holes do occupy the same fundamental plane, and the apparent difference is a result of a small sample size and limited dynamic range. The second is that SMBHs and supermassive black holes each operate under different physical conditions and follow their own relation, and fits to combined samples only appear to produce a single relation because of the large logarithmic range in values. Either empirical result would provide insight to the physics at play.

In this Letter, we report an observational study designed to test which empirical relation is better. We selected a sample of active galactic nuclei (AGNs) with masses in the range that is best suited to make an observational distinction between

the two relations (Section 2.1). We obtained new *Chandra* and Karl G. Jansky Very Large Array (VLA) observations and supplemented these with archival data to put them on the fundamental plane (Sections 2.2 and 2.3). We find that the single plane is a better predictor of the observed radio and X-ray fluxes, and we discuss the implications of our results (Section 3). Throughout this Letter we assume $H_0 = 70 \text{ km s}^{-1} \text{ Mpc}^{-1}$, $\Omega_M = 0.3$, and $\Omega_{\Lambda} = 0.7$.

2. OBSERVATIONS

2.1. Sample Selection

To test whether an SMBH-only relation or an all-black-holes relation was better, we assembled a sample of 13 low-mass AGNs from the sample of Greene & Ho (2007a). Black hole masses (M) come from the virial (i.e., single-epoch) method using broad H α emission lines and an assumed relation between the radius of the broad-line region and continuum luminosity of the AGN, inferred from the broad H α luminosity. The parent sample was defined to have $M < 10^{6.3} M_{\odot}$. Some of the parent sample were flagged with c by Greene & Ho (2007a) to indicate that the broad-line emission may not have been robustly detected. The c-sample sources may therefore have less robust mass estimates. As only one c-sample source is detected in both radio and X-ray, our fundamental-plane analysis and conclusions below are not affected.

Out of 229 low-mass AGNs, we selected 13 for which the X-ray and radio fluxes could be measured in a reasonable exposure as predicted by the Gültekin et al. (2009) fundamental plane. To determine the suitability of potential sources for our new X-ray and radio observations (Sections 2.2 and 2.3), we used information from existing optical observations. For X-ray detectability, we assumed the bolometric luminosities from Greene & Ho (2007a) and bolometric correction from Vasudevan & Fabian (2007). For VLA detectability, we assumed the more conservative of the two Gültekin et al. (2009) fundamental plane predictions.

We included both sources that have VLA FIRST (White et al. 1997) 1.4 GHz detections and those that do not, so as

Table 1
Sample of Small AGN

GH ID	SDSS	z	D_L	$\log(M/M_\odot)$	ΔT_{obs}
47	J082443.28+295923.5	0.025	109	5.70	1890
69	J091449.05+085321.1	0.140	661	6.30	176
87	J101246.49+061604.7	0.078	353	6.22	60
94 ^c	J103234.85+650227.9	0.006	26	5.80	...
101 ^c	J105108.81+605957.2	0.082	373	6.27	...
106	J110501.97+594103.6	0.034	149	5.58	822
119 ^c	J112637.74+513423.0	0.026	114	6.16	...
140 ^c	J121629.13+601823.5	0.060	269	6.18	76
146	J124035.81-002919.4	0.081	368	6.35	2824
158 ^c	J131659.37+035319.8	0.045	199	5.84	226
163 ^c	J132428.24+044629.6	0.021	91	5.81	226
174	J140829.26+562823.5	0.133	626	6.24	68
203	J155909.62+350147.4	0.031	136	6.31	991

Note. — Basic sample properties, including identification from Greene & Ho (2007a), SDSS name, redshift, luminosity distance in Mpc, logarithmic black hole mass in solar units, and time in units of days between radio and X-ray observations if both exist. Only sources with an entry for ΔT_{obs} have both X-ray (new or archival) and radio data for analysis with the fundamental plane, including GH 140 and GH 158, which have only upper limits in X-ray, and GH 174, which has only an upper limit in radio. C-sample sources (Section 2.1) are identified with a superscript c.

not to bias ourselves to those brightest in radio wavelengths. As discussed below, VLA FIRST detection was not a good predictor of 8.5 GHz continuum emission.

To reduce scatter related to source variability, we scheduled *Chandra* and VLA observations contemporaneously. We also used archival X-ray data when possible. Table 1 lists basic properties—including Greene & Ho (2007a) identification number, which we use here—of all low-mass AGNs in our sample. We have updated the masses to use the most recent single-epoch H α scaling relations (Greene & Ho 2005; Bentz et al. 2013; Reines et al. 2013) and to assume a scaling factor of $\varepsilon = 4.3/4$ (Grier et al. 2013), which uses the approximation $V_{\text{FWHM}} = 2\sigma$. This makes a typical difference of < 0.1 dex compared to Greene & Ho (2007a), much smaller than the estimated 0.5 dex systematic uncertainty.

2.2. X-Ray Observations

We used five archival and six new *Chandra* observations to measure X-ray luminosities. For new observations, exposure times were 15 ksec except for the dimmest, GH 140, which had an exposure time of 24 ksec. New *Chandra* observations were observed on the S3 chip of the ACIS-S detector. We re-reduced and re-analyzed the archival data.

Data reduction followed the normal pipeline with the most recent *Chandra* data reduction software package (CIAO version 4.5) and calibration databases (CALDB version 4.5.5). Source regions were circles with radii of 4 or 5 pixels centered on the brightest putative point source consistent with the center of the host galaxy. Given the distances to the host galaxies (Table 1), X-ray binaries are not luminous enough to be a significant source of contamination. Background regions were annuli with inner radii equal to the source region radius and outer radii equal to ~ 30 pixels. We used the specextract tool to create response matrix and ancillary response files and extract source and background spectra.

Spectral fitting was done with the most recent version of Xspec (v12.6.0q; Arnaud 1996). Since we were most interested in the unscattered, intrinsic 2–10 keV flux, we always included a power-law component in our spectral model with Galactic absorption set to the value toward each source (Kalberla et al. 2005). For sources with enough counts, we also included

Table 2
X-ray Observations

GH ID	Obsid	MJD	t_{exp}	$\log(F_X/\text{erg s}^{-1} \text{cm}^{-2})$	Γ
47	504102001	54408	23	$-11.69^{+0.08}_{-0.04}$	2.0 ± 0.2
69	13858	56097	15	-12.43 ± 0.03	1.9 ± 0.1
87	13859	56214	15	-12.63 ± 0.04	2.0 ± 0.2
106	11456	55424	2	$-12.17^{+0.05}_{-0.08}$	$1.6^{+0.2}_{-0.1}$
119	9234	54551	5	< -14.39	1.7
140	13860	56200	24	< -14.05	1.7
146	5664	53428	5	$-12.94^{+0.14}_{-0.09}$	1.7
158	13861	56050	15	< -12.88	1.7
163	13862	56050	15	-12.80 ± 0.07	1.4 ± 0.2
174	13863	56208	15	-12.58 ± 0.03	1.8 ± 0.1
203	11479	55234	2	-11.62 ± 0.03	2.3 ± 0.1

Note. — We provide Obsid, MJD, and exposure time of each *Chandra* observation in ksec along with 2–10 keV flux, and photon index (Γ) with their 1σ uncertainties. When only an upper limit could be determined, we list the 3σ upper limit. Values of Γ without uncertainties were fixed at 1.7. Sources GH 106, GH 119, GH 146, and GH 203 are archival data sets originally analyzed by Dong et al. (2012), Yuan et al. (2014), Greene & Ho (2007b), and Dong et al. (2012), respectively. Values for source 47 are from *XMM-Newton* observations with results due to Ludlam et al. (2014).

redshifted intrinsic absorption. In all cases, as long as the source was detected and total absorption was below $N_H = 10^{20} \text{ cm}^{-2}$, the inferred intrinsic 2–10 keV flux from the power-law component was robust. For sources with low count rates or for which only an upper limit could be determined for the X-ray flux, we held the photon index constant at $\Gamma = 1.7$. Spectral fitting was done with C-stat statistics (Cash 1979). We report 2–10 keV flux and Γ for each source in Table 2. Sources GH 119, and 140 were nondetections; a point source at the location of GH 158 was detected with more than 12 net counts in the 0.5–10 keV band, but it was not enough to constrain the hard flux at the 3σ level.

Source 47 had a 2 ksec archival *Chandra* exposure that showed it likely a Seyfert 2. A 23-ksec *XMM-Newton* archival observation with a high count rate has been looked at in detail by Ludlam et al. (2014). They find that the spectrum of GH 47 is well fitted by a typical type II AGN spectrum consisting of a highly absorbed power-law component, soft, scattered power-law component, and a distant reflection component with prominent narrow Fe K α line. The unabsorbed 2–10 keV flux of the absorbed power-law component is $2.05 \times 10^{-12} \text{ erg cm}^{-2} \text{ s}^{-1}$. We use the *XMM-Newton* measurement for all subsequent analysis.

As a self-consistency check, we calculated Eddington fractions (f_{Edd}) of each source assuming the bolometric correction due to Marconi et al. (2004). Because the X-ray bolometric correction depends on the bolometric luminosity, we use the bolometric luminosity reported in Greene & Ho (2007a). Although using f_{Edd} based on optical emission to estimate f_{Edd} based on X-ray emission is circular, it serves as a check for self-consistency. Using a constant bolometric correction of 20 instead of our adopted circular method does not make a large difference. We plot the X-ray f_{Edd} as a function of the optically determined f_{Edd} in Figure 1. The agreement between the two estimates shows self-consistency.

2.3. Radio Observations

Radio data presented in this Letter come from new VLA observations, taken at 8.4 GHz with 2 GHz bandwidth in the A configuration. The data were from two programs targeting low-mass AGNs, one selecting from those with VLA FIRST detections, one from those without. All observations began

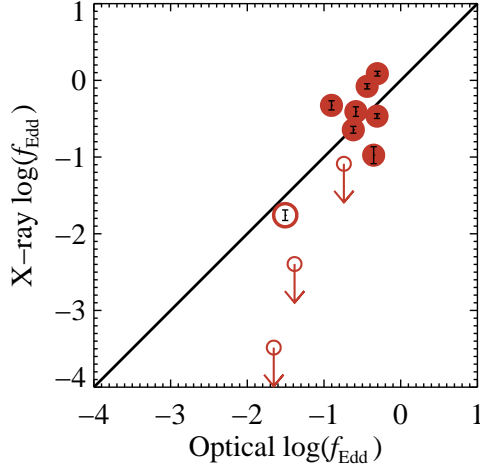


Figure 1. Comparison of f_{Edd} estimates. The abscissa shows f_{Edd} determined by Greene & Ho (2007a) from optical spectra. The ordinate shows f_{Edd} determined from 2–10 keV luminosities and bolometric corrections due to Marconi et al. (2004). Since the X-ray bolometric corrections depend on the bolometric luminosity, we use L_{bol} as determined by Greene & Ho (2007a), which serves as a check for self-consistency. Open circles indicate c-sample sources. The error bars come from the uncertainty on the X-ray flux only, and the line shows equality. There is generally good agreement, and the points above $f_{\text{Edd}} = 1$ are consistent with sub-Eddington accretion when uncertainties in black hole mass and bolometric correction are taken into account.

with a scan on a flux calibrator. 3C 286 was used for all observations, except GH 57 and GH 69, for which 3C 147 was used. The flux calibrator was followed by a phase calibrator (Table 3). Then we cycled between the source and the phase calibrator for the remaining duration of the scan.

Flagging and reduction of VLA data followed the standard pipeline using CASA version 4.0.1. We calibrated fluxes based on the most recent calibration models, implemented phase corrections, and then calibrated the bandpass. We averaged the data in bins in time by 30 s and in frequency by eight channels. Each frequency was converted into an image and processed with the CLEAN algorithm separately with a maximum of 5000 iterations, a gain of 0.1, and natural weighting. The processing used the full width of the 512×512 image at a resolution of $0''.05$ and typically stopped at a threshold of 0.05 mJy.

The resulting processed images were then inspected for emission at the location of the AGN. In 10 of the 12 sources, there was an unambiguous, unresolved point source at the coordinates of the galaxy center. We attribute this flux to the AGN. For these detected sources, we calculated the flux density by fitting a two-dimensional Gaussian to the point source in a 20×20 pixel box and using the total flux reported by the imfit tool. Uncertainties in flux were calculated as the quadrature sum of uncertainty in the fit and rms noise of the image. All detections were highly significant ($> 10\sigma$). The final flux densities we report (Table 3) are from the channel centered at 8.5 GHz with an additional 5% uncertainty to account for absolute flux calibration. Non-detections are reported as 3σ upper limits of the rms noise of the image.

Detection of the sources in the VLA FIRST survey was not a good predictor of AGN radio emission. The two non-detections are detected in VLA FIRST, indicating that the 1.4 GHz VLA FIRST detection is not associated with AGN activity. All sources without detection at 1.4 GHz were detected at 8.5 GHz. For the detected sources, we attempted to constrain the

spectral index, α ($S_\nu \propto \nu^{-\alpha}$), by fitting a power law to the fluxes across the entire bandpass of the radio observations, but the relatively large uncertainties meant that we only had a weak constraint. All measurements were consistent with $\alpha = 0.7$, which we assume for subsequent analysis.

3. ANALYSIS AND DISCUSSION

Our primary analysis is to compare these low-mass AGNs with the earlier sample of SMBHs with dynamical masses on the fundamental plane. As mentioned in Section 2.1, we update the Greene & Ho (2007a) masses using the most recent H α AGN-mass scaling relations and adopt conservative uncertainties of 0.5 dex. The uncertainty in mass is much larger than the statistical uncertainties in the H α luminosity and line-width measurements, the uncertainties in the best-fit AGN-mass scaling relations, and the intrinsic scatter in the scaling relations. The larger uncertainty, however, should encompass systematic uncertainties in mass estimation such as extrapolation of scaling relations to low masses (e.g., Greene et al. 2010), linking H β scaling relations to H α scaling relations, and imperfect decomposition of narrow lines and broad lines, which may be especially difficult for narrow-line Seyfert 1 AGNs (Denney et al. 2009).

We calculate 5 GHz radio luminosities from our measured 8.5 GHz flux densities assuming a spectral index of $\alpha = 0.7$. Note that $L_R \equiv \nu L_\nu$, whereas the 2–10 keV X-ray luminosity, L_X , is a bandpass luminosity.

From the 13 sources in Table 1, we have usable data in both X-ray and radio for 10, including 3 sources with upper limits on one of the two quantities. We compare these data to the two fundamental-plane fits in Figure 2 and find that they are better predicted by the universal (all black holes) fit. The low-mass AGNs are inconsistent with the SMBH-only relation, having higher L_R , lower L_X , and/or lower M than predicted. Compared to the universal relation, the low-mass AGNs are within the scatter.

The low-mass AGNs are slightly but systematically offset from the better-fitting SMBH-only plane in one direction (Figure 2, right panel). The median deviations in the L_R , M , and L_X directions are 0.63, -0.81 , and -0.95 dex, respectively. The magnitude of these deviations is within the scatter, but of seven sources with both X-ray and radio detections, six lie to one side of the plane. If an individual source is equally likely to lie on either side of the plane, the probability of six or more out of seven lying on the same side (high or low, i.e., two-sided) by chance is 0.125. If we exclude the c-sample source GH 163 from this calculation, then chance alignment for five of six sources would happen 0.219 of the time. This is only weak evidence of a systematic deviation, but we briefly speculate on potential reasons if this trend were to continue with more data. Despite this speculation, below we conclude that the low-mass AGNs are consistent with the full fundamental plane, which we argue should be considered the better model.

Because black hole mass is a notoriously difficult quantity to estimate and is the only indirect quantity considered, we give it special attention. The Greene & Ho (2007a) sample is selected for broad H α lines with small FWHM. It is possible, but not certain, that broad emission lines come from the base of a disk wind (e.g., Kollatschny & Zetzl 2013) with predominantly rotational motions. The resulting FWHM measurement would be subject to orientation effects that could lead to a preferential selection of face-on inclinations and underestimation of the true mass. This possibility is supported by the LAMP 2008 campaign’s finding that lower inclination objects return larger

Table 3
VLA Observations

GH ID	SB ID	MJD	Cal.	t_{exp}	Beam Size	S_{ν} /mJy	rms/mJy
47	12097202	56298	J0830+2410	59.5	$0''.37 \times 0''.28$	0.93 ± 0.05	0.014
69	12452868	56274	J0914+0245	34.7	$0''.36 \times 0''.26$	0.60 ± 0.03	0.015
87	12465022	56274	J1008+0730	33.2	$0''.42 \times 0''.26$	0.42 ± 0.03	0.022
94	12469924	56274	J0958+6533	33.9	$0''.32 \times 0''.25$	< 0.29	0.087
101	12118330	56243	J1033+6051	57.6	$0''.33 \times 0''.25$	0.54 ± 0.03	0.012
106	12117646	56246	J1110+6028	57.6	$0''.31 \times 0''.25$	1.10 ± 0.06	0.014
140	12465449	56276	J1217+5835	33.8	$0''.28 \times 0''.24$	0.37 ± 0.03	0.018
146	11470757	56252	J1229+0203	56.3	$0''.42 \times 0''.26$	0.45 ± 0.03	0.017
158	12465639	56276	J1256-0547	30.9	$0''.30 \times 0''.24$	0.57 ± 0.03	0.023
163	12465813	56277	J1347+1217	32.1	$0''.49 \times 0''.26$	0.50 ± 0.03	0.022
174	12469748	56276	J1419+5423	34.1	$0''.37 \times 0''.24$	< 0.10	0.028
203	12118194	56225	J1602+3326	57.4	$0''.27 \times 0''.26$	0.58 ± 0.04	0.015

Note. — VLA scheduling block identification, MJD of observation, gain calibrator, time on source in minutes, size of synthesized beam, flux density of source, and rms of map in mJy. All observations used 3C286 for flux calibration and bandpass calibration except for GH 47 and GH 69, which used 3C147. The flux density uncertainty includes a 5% uncertainty in absolute flux calibration, which dominates the total uncertainty. Upper limits are 3σ values.

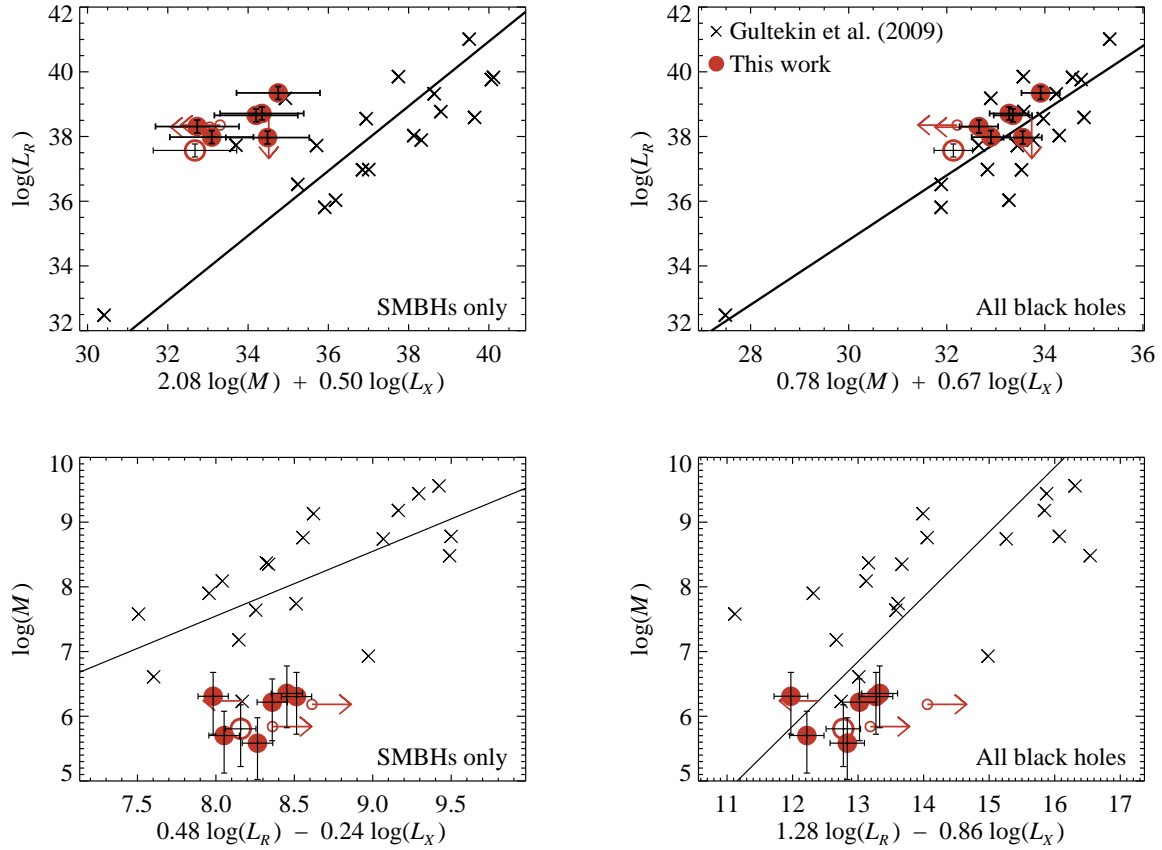


Figure 2. New data for the current sample of small AGNs (red circles) and for SMBHs with dynamically determined black hole masses (black crosses) due to Gültekin et al. (2009). Open circles indicate sources from the Greene & Ho (2007a) c-sample. Top panels have L_R as the dependent variable, and bottom panels have M as the dependent variable. The left panels are projected to display the edge-on view of the best fit to SMBHs with dynamical masses only, and the right panels for both stellar-mass and SMBHs with dynamical masses. Fits do not include low-mass AGNs, and thus we may compare the new, low-mass data to the values predicted by the fitted relations. Low-mass AGNs are inconsistent with the prediction of the left panels and consistent with the prediction of the right panels.

virial coefficients (Pancoast et al. 2013).

Several other lines of evidence, however, point to, on average, accurate mass estimation. First, reverberation mapping of GH 126 indicates a small mass in agreement with the $H\alpha$ single-epoch estimate (Rafter et al. 2011). Second, the expected black hole mass based on host galaxy stellar velocity dispersion generally agrees with the single-epoch estimates (Xiao et al. 2011), though megamaser measurements of black hole mass in small galaxies show that the masses can be much smaller than predicted by velocity dispersion (Greene et al. 2010) and low-mass AGNs appear undermassive relative to their bulge luminosity (Jiang et al. 2011a). Given that many of the host galaxies are likely to be pseudobulges (Jiang et al. 2011b), black hole mass–host galaxy property scaling relations may not apply to the majority of these galaxies (Kormendy et al. 2011; Greene et al. 2010). Finally, Ludlam et al. (2014) recently found that the X-ray variability of a different sample of Greene & Ho (2007a) AGNs is as expected for low-mass sources. Given the above evidence, we find it unlikely that underestimated masses are the cause of the offset.

Another possibility is that the offset results from different accretion–jet interactions. The data are not conclusive, but X-ray properties of AGNs may depend on black hole mass (Desroches et al. 2009; Dong et al. 2012). Given the inferred near-ultraviolet luminosity of these low-mass AGNs, their spectral index between 2500 Å and 2 keV (α_{OX}) may be flatter than expected, and their 2 keV X-ray emission sometimes weaker than expected, though selection effects may complicate the issue. This may be evidence of slim-disk accretion, lack of a Comptonizing corona, or high intrinsic absorption. Thus the 2 keV X-ray emission of low-mass AGNs may not be as reliable a probe of accretion power as it is in higher mass AGNs. If the difference were a result of a lack of a Comptonizing corona, then this would lead to an absence of 2–10 keV flux, which we assume is from inverse Compton scattering. Rather, we observe X-ray flux levels that are consistent with expectations based on the accretion rate and bolometric corrections (Figure 1). If the difference in 2 keV luminosity is, instead, a result of high intrinsic absorption of any form, our conclusions should be unaffected owing to our use of hard flux and deeper observations.

Based on the relatively small offset, the reliability of 2–10 keV flux measurements in the face of absorption, and the low significance of a possible offset of the low-mass points from the fundamental plane, we conclude that low-mass AGNs do in fact follow the full $M-L_R-L_X$ plane. Our results suggest that stellar-mass black holes and supermassive black holes follow the same relation. A similar test using the most massive black holes would provide additional support.

Given the low mass and relatively high accretion rates here, we can now state with confidence that (1) it is appropriate to use the fundamental plane to estimate SMBH masses smaller than $\sim 10^7 M_\odot$ (e.g., Reines et al. 2011), (2) it is possible to use the fundamental plane to test for intermediate mass black

holes (e.g., Mezcua et al. 2013), and (3) it is possible to use the fundamental plane to estimate black hole masses at high accretion rates (e.g., Miller & Gültekin 2011).

We thank Jenny Greene for a valuable referee report and Elena Gallo for helpful comments. K.G. acknowledges support provided by NASA through Chandra Award G02-13111X (*Chandra X-Ray Observatory* operated by NASA under contract NAS8-03060). Results reported here are based on new and archival *Chandra* data. We used NED, ADS, and CIAO and are grateful.

REFERENCES

- Arnaud, K. A. 1996, in *Astronomical Society of the Pacific Conference Series* 101, *Astronomical Data Analysis Software and Systems V*, ed. G. H. Jacoby & J. Barnes, 17
- Bentz, M. C., et al. 2013, *ApJ*, 767, 149
- Cash, W. 1979, *ApJ*, 228, 939
- Denney, K. D., Peterson, B. M., Dietrich, M., Vestergaard, M., & Bentz, M. C. 2009, *ApJ*, 692, 246
- Desroches, L.-B., Greene, J. E., & Ho, L. C. 2009, *ApJ*, 698, 1515
- Dong, R., Greene, J. E., & Ho, L. C. 2012, *ApJ*, 761, 73
- Falcke, H., Kording, E., & Markoff, S. 2004, *A&A*, 414, 895
- Gallo, E., Fender, R. P., & Pooley, G. G. 2003, *MNRAS*, 344, 60
- Gallo, E., Miller, B. P., & Fender, R. 2012, *MNRAS*, 423, 590
- Greene, J. E., & Ho, L. C. 2005, *ApJ*, 630, 122
- . 2007a, *ApJ*, 670, 92
- . 2007b, *ApJ*, 656, 84
- Greene, J. E., et al. 2010, *ApJ*, 721, 26
- Grier, C. J., et al. 2013, *ApJ*, 773, 90
- Gültekin, K., Cackett, E. M., Miller, J. M., Di Matteo, T., Markoff, S., & Richstone, D. O. 2009, *ApJ*, 706, 404
- Jiang, Y.-F., Greene, J. E., & Ho, L. C. 2011a, *ApJ*, 737, L45
- Jiang, Y.-F., Greene, J. E., Ho, L. C., Xiao, T., & Barth, A. J. 2011b, *ApJ*, 742, 68
- Kalberla, P. M. W., Burton, W. B., Hartmann, D., Arnal, E. M., Bajaja, E., Morras, R., & Pöppel, W. G. L. 2005, *A&A*, 440, 775
- Kollatschny, W., & Zetzl, M. 2013, *A&A*, 551, L6
- Kormendy, J., Bender, R., & Cornell, M. E. 2011, *Nature*, 469, 374
- Ludlam, R. M., Cackett, E. M., Gültekin, K., & Miniutti, G. 2014, in preparation
- Marconi, A., Risaliti, G., Gilli, R., Hunt, L. K., Maiolino, R., & Salvati, M. 2004, *MNRAS*, 351, 169
- Merloni, A., Heinz, S., & Di Matteo, T. 2003, *MNRAS*, 345, 1057
- Mezcua, M., Farrell, S. A., Gladstone, J. C., & Lobanov, A. P. 2013, *MNRAS*, 436, 1546
- Miller, J. M., & Gültekin, K. 2011, *ApJ*, 738, L13
- Pancoast, A., Brewer, B. J., Treu, T., Park, D., Barth, A. J., Bentz, M. C., & Woo, J.-H. 2013, (arXiv:1311.6475)
- Rafter, S. E., Kaspi, S., Behar, E., Kollatschny, W., & Zetzl, M. 2011, *ApJ*, 741, 66
- Reines, A. E., Greene, J. E., & Geha, M. 2013, *ApJ*, 775, 116
- Reines, A. E., Sivakoff, G. R., Johnson, K. E., & Brogan, C. L. 2011, *Nature*, 470, 66
- Vasudevan, R. V., & Fabian, A. C. 2007, *MNRAS*, 381, 1235
- White, R. L., Becker, R. H., Helfand, D. J., & Gregg, M. D. 1997, *ApJ*, 475, 479
- Xiao, T., Barth, A. J., Greene, J. E., Ho, L. C., Bentz, M. C., Ludwig, R. R., & Jiang, Y. 2011, *ApJ*, 739, 28
- Yuan, W., Zhou, H., Dou, L., Dong, X.-B., Fan, X., & Wang, T.-G. 2014, *ApJ*, 782, 55